# Single-Walled Tubulin Ring Polymers

Hacène Boukari,[1] Dan L. Sackett,[1] Peter Schuck,[2] Ralph J. Nossal[1]

[1] *Laboratory of Integrative and Medical Biophysics, NICHD, National Institutes of Health, Bethesda, MD 20892*

[2] *Protein Biophysics Resource, NIBIB, National Institutes of Health, Bethesda, MD 20892*

*Received 26 March 2007; revised 27 April 2007; accepted 27 April 2007*
*Published online 4 May 2007 in Wiley InterScience (www.interscience.wiley.com). DOI 10.1002/bip.20752*

**ABSTRACT:**

*An unusual class of nanoscopic, ring-shaped, single-walled biopolymers arises when αβ-tubulin is mixed with certain small peptides obtained from various marine organisms and cyanobacteria. The single-ring structures, whose mean molecular weight depends on the specific peptide added to the reaction mixture, usually have sharp mass distributions corresponding, e.g., to rings containing eight tubulin dimers (when the added peptide is cryptophycin) and 14 dimers (e.g., with dolastatin). Although the ring-forming peptides have been shown to possess antimitotic properties when tested with cultured eukaryotic cells (and thus have generated considerable interest as possible agents to be used in the treatment of cancer), it is not our intention to extensively discuss the potential pharmacological properties of the peptides. Rather, we will review the polymeric structures that form and illustrate how certain physical techniques can be used to characterize their properties and interactions. The nanoscopic size and particular geometry of the individual rings make them appropriate targets for scattering and hydrodynamic techniques that provide details about their structure in solution, but it is necessary to relate measured data to postulated structures by nontrivial, albeit straight-forward, mathematical, and computational means. We will discuss how this is done when one uses such methods as small angle neutron scattering, dynamic light scattering, fluorescence correlation spectroscopy, and sedimentation velocity measurements. Moreover, we show that, by using several techniques, one can eliminate degeneracy to provide better discrimination between model structures. © 2007 Wiley Periodicals, Inc.† Biopolymers 86: 424–436, 2007.*

*Keywords: tubulin rings; small-angle neutron scattering; fluorescence correlation spectroscopy; dynamic light scattering; hydrodynamic modeling*

*This article was originally published online as an accepted preprint. The "Published Online" date corresponds to the preprint version. You can request a copy of the preprint by emailing the Biopolymers editorial office at biopolymers@wiley.com*

*Correspondence to:* Hacène Boukari; e-mail: boukarih@mail.nih.gov
Contract grant sponsor: National Institute of Child Health and Human Development, NIH

WILEY InterScience® DISCOVER SOMETHING GREAT

© 2007 Wiley Periodicals, Inc. †This article is a US Government work and, as such, is in the public domain in the United States of America.

## INTRODUCTION

Tubulin (Tu) is a ubiquitous protein in the cytoplasm of eukaryotic cells.[1] It is a heterodimer composed of two isotypes (α and β), differing in amino-acid sequence but similar in shape (width: 4.6 nm, height: 4.0 nm, depth: 6.5 nm) and molecular weight (∼50 kDa).[1,2] The αβ-tubulin dimer is the building block of microtubules, which are long hollow cylinders that mediate several critical cellular functions.[1,3] Several other biopolymeric structures can also be assembled from tubulin. Examples are GDP-Mg double-walled tubulin rings, (2-stacked rings),[4,5] and vinblastine-induced helical tubulin filaments.[6] Recently, various small peptides have been shown to induce self-assembly of tubulin complexes into single-walled rings such as that shown in Figure 1.[7–12] We have investigated the assembly and structure of these rings under various experimental conditions.[10–12] One motivation has been the potential use of these

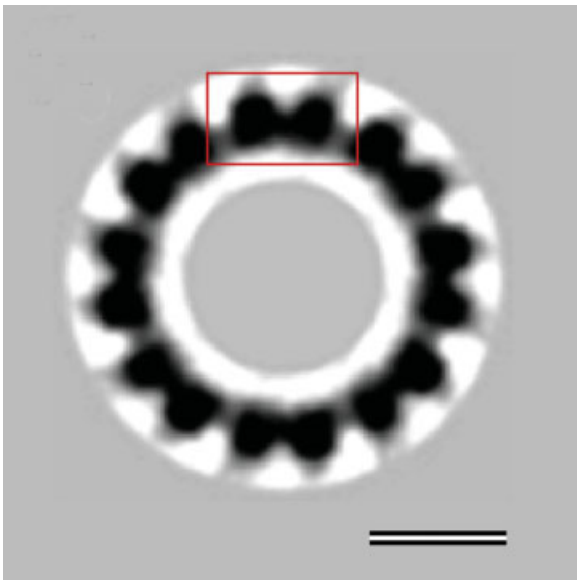

**FIGURE 1** Averaged cryo-electron microscopy image of a cryptophycin-induced tubulin ring [see Ref. 8]. The bar represents 10 nm.

peptides as antimitotic drugs, a goal currently being pursued by numerous research laboratories and pharmaceutical companies.[7,13–17] However, these tubulin rings are also of interest in both fundamental research and applied engineering. They can be used, for example, as models for understanding the self-assembly processes of other biopolymeric closed structures[18–29] or be considered as templates for producing ring structures with different materials as reported in Ref. 30.

In the present paper we review our results of various measurements on rings induced by the interactions of tubulin with either cryptophycin-1 (MW = 654 Da, isolated from cyanobacteria[7,13]) or dolastatin-10 (MW = 785 Da, isolated from shell-less mollusks[7,15,17]). These ring structures have nanoscopic dimensions (∼24 and 44 nm diameter for cryptophycin-tubulin and dolastatin-tubulin rings, respectively), and are amenable to study by electron microscopy (EM), small-angle neutron scattering (SANS), dynamic light scattering (DLS), fluorescence correlation spectroscopy (FCS), and sedimentation velocity (SV). Although the mentioned techniques exploit different physical mechanisms (scattering, hydrodynamics, fluorescence) for probing the nanoscopic structure of the biopolymers, each provides complementary quantitative information. We note that besides EM, which provides a direct image of the rings, the data obtained from the other less-intrusive techniques need to be inverted in order to extract the appropriate structural information. Here, we have used two simple structural models, the NXbead ring (Figure 2a) and the NX21-minibead ring (Figure 2b), which were inspired by EM micrographs of these rings. (See below for explanation of the models.)

We find that analysis of the various measurements yields consistent results. The Cryptophycin-Tubulin (CrTu) and the Dolastatin-Tubulin (DoTu) rings, which were prepared under similar solution conditions, show different structural characteristics, although bioassays[7] and molecular-dynamics-simulations/molecular-docking studies[31] indicate that both peptides bind to the same site, an area that overlaps with Vinca alkaloid binding site and which is known as the "Vinca domain". The CrTu rings appear rigid, have well-defined circular geometry, are monodisperse in size (eight dimers per ring, close to 24 nm diameter), and are stable against dilution to concentrations as low as one nanomolar. In contrast, the DoTu rings are composed predominantly of 14 tubulin dimers and have a diameter of about 44 nm and, at micromolar concentrations, appear to interact with each other to form large macrostructures.

Several predictions, mostly based on computer simulations, have been published on the structure and dynamics of ring polymers.[32–34] However, finding a model system to test these theories has eluded experimentalists so far. Until now, there has been no thorough experimental study of circular ring polymers because of difficulties in synthesizing samples

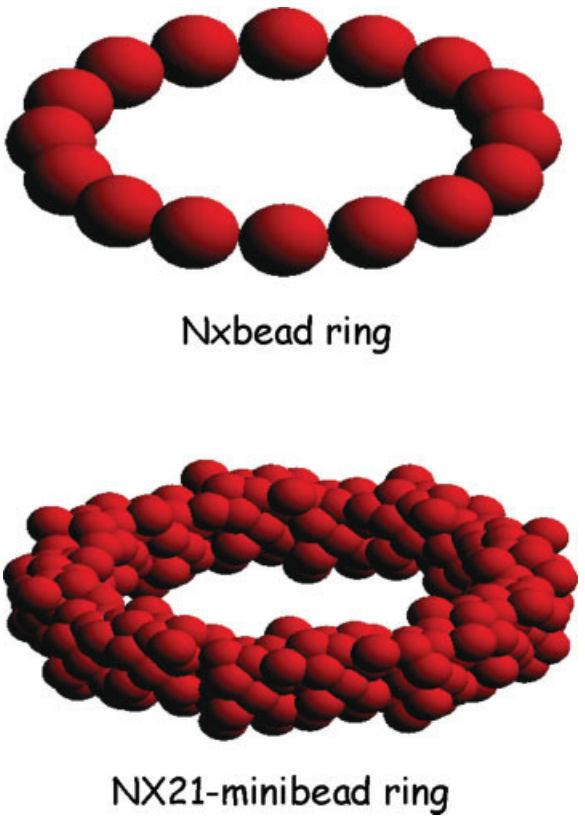


**FIGURE 2** Structural models used to describe cryptophycin-induced rings. (a) the NXbead model; (b) the NX21-minibead model of Figure 1.

appropriate for experimental studies.[32] Because of their specific attractive interactions, the CrTu and DoTu complexes assemble into geometrically well-defined ring structures, unlike nonspecific interactions that generally lead to amorphous aggregates. Here, we emphasize that, in contrast to ring polymers described in the polymer science literature,[32–34] CrTu and DoTu rings have relatively thick walls that make them look like toroids. Moreover, they are polyelectrolytes. It is important to note that various closed polymeric structures have been observed in biological systems with sometimes critical functional roles. Examples are bacteriophage DNA condensed with multivalent cations,[18] hexameric protein complexes involved in DNA replication,[20] assemblies of sRNA binding proteins,[19] dynamin oligomers,[22] clathrin baskets involved in endocytosis,[23,24] virus capsids,[25,26] and COPII cages.[27–29]

## SAMPLES

The peptide (cryptophycin or dolastatin) and tubulin (rat or bovine MAP-free tubulin) samples were prepared in 0.1*M* PIPES, pH 7.0, or 0.1 MES, pH 6.9, both containing 1 m*M* $MgCl_2$. To ensure the formation of the rings we added tubulin ([Tu] = 3 $\mu M$ for DLS and [Tu] = 40 $\mu M$ for SANS) and excess of the peptide ([peptide] = 5 and 50 $\mu M$, respectively) to the buffer. At these concentrations, ring polymerization starts immediately following the addition of the components to the buffer. The actual sample volumes depended on the experiment, as will be described later.

## METHODS AND RESULTS

SANS, DLS, SV, and FCS have their own advantages as well as limitations. For SANS one should expect the scattering profile of the rings to contain maxima and minima in a range detectable by the technique. With further modeling the precise positions of these maxima and minima can be directly related to the actual diameter and shape of the rings. However, because proteins are generally poor scatterers of neutrons, SANS requires a relatively large amount of materials (~40 $\mu M$ for the present studies) to obtain good signal-to-noise. Further, SANS instruments, which are part of large government facilities, are not easily accessible. Typically, a research proposal must be submitted and subsequently reviewed in order to acquire beam time (2–3 days at most). Thus, it is important that preliminary, and sometimes extensive, investigations (chemical analysis, structural characterization, etc.) on the system be done in the laboratory prior to justify SANS use. In contrast, DLS and SV are well-established techniques with instruments becoming standard tools in various biochemical and biophysical laboratories. For reliable data, typical DLS and SV experiments require volumes of a few hundred microliters at micromolar concentration. As will be discussed below, the main difficulty in these experiments is the interpretation of the primary data (correlation functions and sedimentation profiles), which need to be inverted into meaningful, and accurate, size distributions. This inversion could be marred by the presence of dust particles or unwanted aggregates. Here, SV provides an advantage as these particles or aggregates are removed by the centrifugation force, which is set by the chosen rotation speed, allowing one to focus on a specific range of sedimentation values.

FCS is a relatively new technique and is undergoing major growth in the number of applications. Its main advantages are fluorescence specificity, low nanomolar concentrations of materials of fluorescent sample (although total concentration of sample maybe increased to any desired level by addition of nonfluorescent sample), and low volume requirement (as low as 10 $\mu$l). However, care must be taken in the interpretation and analysis of the main data (correlation functions), a task that often faces the same limitations as those of DLS data. That is, the inversion of the correlation into actual distribution of sizes and assessment of the accuracy of the obtained distribution often is difficult. In our ring system, some of these limitations are overcome by using ratios of the properties of unpolymerized tubulin and those of closed polymerized tubulin rings, as demonstrated in Ref. 11.

### Structural Modeling and Calculations

Cryoelectron microscopy provides structurally averaged, "real-space" images of the rings similar to that shown in Figure 1. In contrast, analysis by SANS, DLS, FCS, and SV requires a priori structural models whose calculated physical properties—in particular, scattering cross-sections and/or hydrodynamic coefficients—are then fit to, or compared with, the data in a consistent way.

We first modeled tubulin monomers as spherical beads, in which case the principal ring building block, the $\alpha\beta$ heterodimer, is represented as a dimer of beads and the CrTu and DoTu rings are rigid planar structures constructed from *N* contiguous beads (We refer to these as "NXbead rings", see Figure 2a.). We used the generic computer code HYDRO[35,36] to calculate scattering profiles for these structures. However, although we employ HYDRO to calculate the hydrodynamic properties of more complicated structures (see below), analytical expressions are available for hydrodynamic parameters of these simplified models. In particular, the diffusion coefficient of a dimer of beads, *D*(dimer), can be related to that of

a monomer bead by: $D$(dimer) = $D$(bead)/1.43, where Stokes' law is assumed for an individual bead.[37] For the rings, we adapted expressions obtained by Yamakawa and Yamaki, who derived closed-form expressions for the translational diffusion coefficient of polygonal arrays of beads as a function of the number of beads.[38] Yamakawa and Yamaki used the modified Riseman-Kirkwood approximation to determine the translational diffusion tensor and showed that the tensor contains two diffusion coefficients, $D_1$ along the plane of the ring and $D_2$ perpendicular to the plane [see Eqs. (70) and (71) in Ref. 38], according to which an average diffusion coefficient was derived to be $D_N = (2D_1 + D_2)/3$. From $D_N$ one can compute the corresponding hydrodynamic diameter, $d_{HN,}$ of the NXbead ring using the Stokes-Einstein relation [see Eq. (3) below].

A more refined model of the tubulin monomer is the 21-minibead representation determined by Diaz et al. from small-angle X-ray scattering data on double-walled tubulin rings.[4,5] The corresponding "NX21-minibead ring" is constructed by juxtaposing N X 21-minibead monomers, yielding the structure shown in Figure 2b. Since the shape and dimensions of the monomer are fixed, $N$ is the only variable in the model. For these complex structures we used the code HYDRO to calculate the hydrodynamic properties of these complex entities[35,36] in addition to their scattering profiles. HYDRO, which takes into account the hydrodynamic interactions between the various surfaces of irregularly shaped objects, is a powerful tool for examining nanoscopic biological polymers. Calculations based on this code have been shown to agree well with theoretical results for several classes of rigid bodies for which analytical expressions exist. Another computer code, ZENO, has been recently released and shown to also calculate the translational diffusion coefficients of given macromolecular objects with accuracy similar to that of HYDRO.[37,39]

## Small-Angle Neutron Scattering

The basic formalism of SANS is described elsewhere.[40] Typically, the measurement consists of determining the intensity of the neutrons scattered at various angles, {θ}, relative to the direction of an incident neutron beam. The measured intensity profile, $I(Q)$, is then plotted as a function of the amplitude of the wavevector, $Q$, defined as $Q = (4\pi/\lambda)\sin(\theta/2)$, $\lambda$ being the wavelength of the neutron beam. In our work, $I(Q)$ is compared with scattering intensities calculated from the two structural models shown in Figures 2a and 2b. The SANS measurements were carried out at the 30m SANS instrument at the National Center for Neutron Research (NCNR) at the National Institute of Standards and Technology (NIST) in Gaithersburg, Maryland (USA). Details on the specifications and operations of the instrument are reported in Refs. 41 and 42.

***SANS: Cryptophycin-Tubulin Solutions.*** We measured SANS profiles of CrTu samples at several temperatures (10–33°C) in order to assess the effects of temperature on the ring formation and stability. We find no observable effects, in contrast to microtubules which depolymerize when the temperature is lowered. In Figure 3a we show the scattering profile obtained from CrTu samples at 33°C. Several peaks or bands can be readily discerned. In the same figure we plot calculated scattering profile of the NXbead model (see Figure 2a) where $N = 16$ and $a = 4.75$ nm. This bead diameter ($a = 4.75$ nm), obtained by optimizing the fit to the data, is very close to the geometrical mean value (4.8 nm) derived from the known dimensions of a tubulin monomer (width = 4.6 nm, height = 4.0 nm, depth = 6.5 nm).[2] However, as shown in Figure 3a, the 21-minibead representation of the ring (16 × 21-minibead, Figure 2b) yields better agreement with the measured profile: the peaks derived from this model align well with the measured ones and the trend in the decrease of the profile at high $Q$ is well captured. In both models, $N = 16$ is sufficient to describe the scattering data. That is, the ring is composed of eight tubulin dimers.

***SANS: Dolastatin-Tubulin Solutions.*** The scattering profile of DoTu differs from that of CrTu although the samples were prepared at close to equal concentrations under the same conditions. Contrast the measured profile of the DoTu shown in Figure 3b with that of the CrTu plotted in Figure 3a. In Figure 3b we plot calculated scattering profiles of a 28Xbead ring and a 28 × 21-minibead ring (we have taken $N = 28$ (i.e. 14 tubulin dimers) as suggested in[7]). For consistency we have used the bead diameter ($a = 4.75$ nm) as derived for the CrTu rings in Figure 3a. Although the models predict most of the peaks in the $Q$-range of interest, they cannot account for the observed amplitudes and for the locations of the first two peaks. It is rather intriguing that some of the calculated peaks are shallower than the experimental peaks. This result is opposite to expectations for idealized rings since the observed scattering profiles should be smeared by various experimental effects (beam size, detection resolutions, etc.) and sample-related imperfections (impurities, etc.), resulting in attenuation of the peaks. Instead of isolated rings, a columnar structure formed by stacking the primary rings provides a better description of the data, which is also consistent with aggregation/polymerization visually observed in DoTu samples. To illustrate the effect of ring stacking on scattering, we plot in Figure 3c calculated profiles of columns

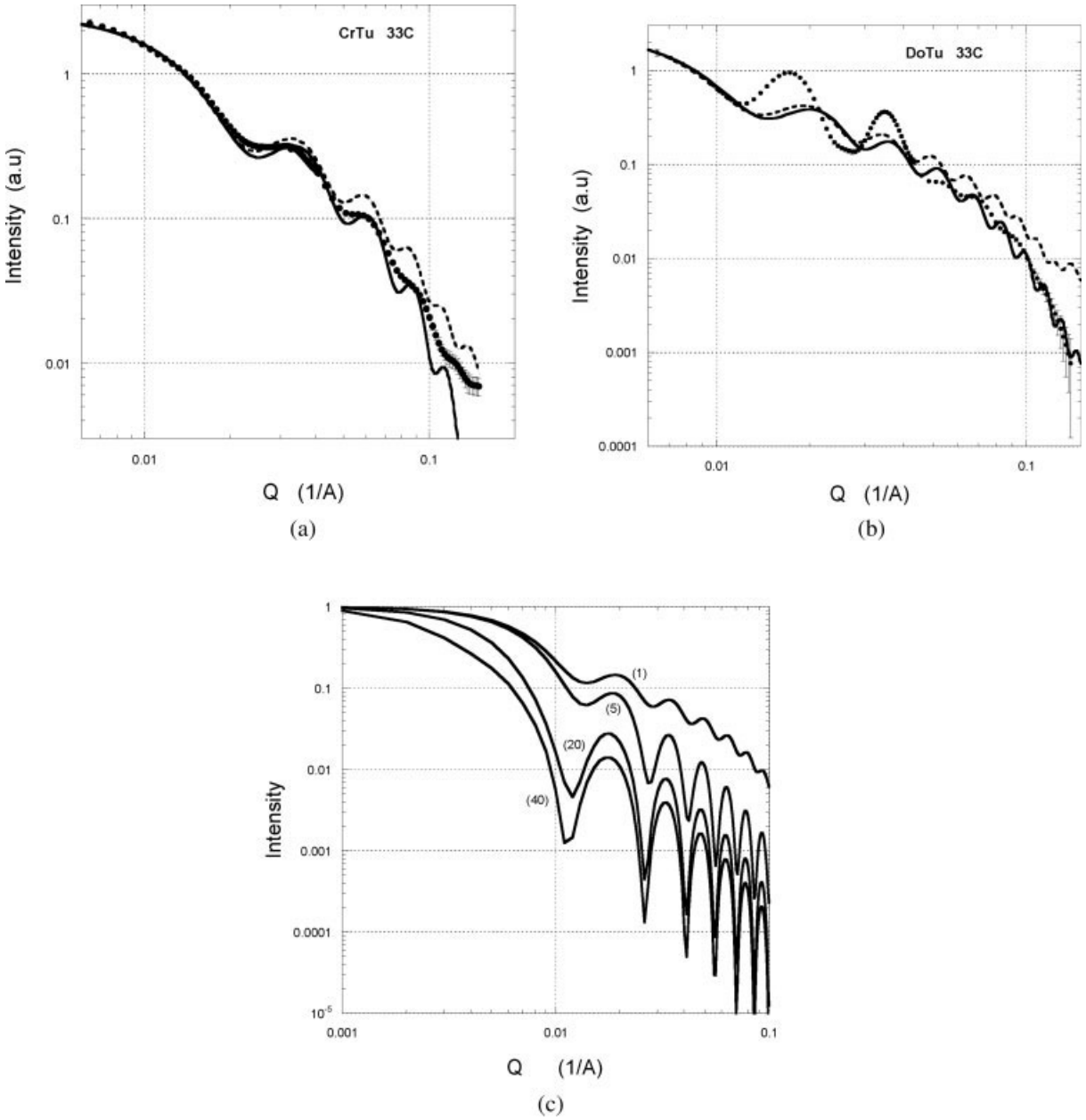


**FIGURE 3** (a) SANS profiles of cryptophycin-tubulin samples: (•) measured profile at 33°C; (--) calculated and scaled profile for a 16Xbead ring with a bead diameter of 4.75 nm; and (–) calculated and scaled profile for a 16 × 21-minibead ring (see Figure 2 and text). Note the four peaks or bands in the scattering profiles. (b) SANS profiles of dolastatin-tubulin samples: (•) measured profile at 33°C, (--) calculated profile for a 28Xbead ring with a bead diameter of 4.75 nm, and (–) calculated profile for a 28 × 21-minibead ring (see Figure 2 and text). Contrast the measured pronounced peaks with those calculated. (c) Calculated scattering profiles of stacked 28Xbead rings are plotted as a function of the amplitude of the scattering vector, *Q*. Note the shift of the peaks to lower *Q*-values, as well as the sharpening of the peaks as the number of stacked rings is increased. Each curve is labeled with the number of stacked rings.

made with different numbers of 28Xbead rings. As the number of stacked rings is increased, the peaks shift to smaller *Q*-values and become sharper.[3,12] The results of these calculations are consistent with the observed additional assembly into large macrostructures and the resulting sharpening of the peaks in the measured profiles.

## Dynamic Light Scattering

The basic principles of DLS have been discussed in several reviews and books.[43,44] Briefly, the main measurement in DLS is the intensity–intensity time correlation function, $C(\tau)$, defined for a stationary process as:

$$C(q,\tau) = \frac{\langle i(q,t)i(q,t+\tau)\rangle}{\langle i(q,t)\rangle^2} = 1 + |\beta g(q,\tau)|^2 \qquad (1)$$

where $t$ denotes time, $i(q,t)$ is the scattered intensity at the scattering vector $q = (4\pi n/\lambda)\sin(\theta/2)$, and $n$, $\lambda$, and $\theta$ are the index of refraction of the solution, the wavelength of the laser beam, and the scattering angle, respectively. $\beta$ is the coherence factor ($\leq 1$), and $g(q,t)$ is the dynamic structure factor. The angular brackets in Eq. (1) denote an ensemble average, but because of the ergodicity of the system the latter can be replaced by a time average, the quantity directly obtained from a single DLS measurement.

For monodisperse noninteracting Brownian scatterers,

$$g(q,\tau) \sim \exp(-Dq^2\tau), \qquad (2)$$

where $D$ is the translational diffusion coefficient. Further, the Stokes-Einstein expression,

$$D = \frac{k_B T}{3\pi\eta d_H} \qquad (3)$$

relates the diffusion coefficient to the hydrodynamic diameter, $d_H$. In Eq. (3), $k_B$ is the Boltzmann constant, $T$ the temperature of the sample in degrees Kelvin, and $\eta$ the viscosity of the buffer. For polydisperse noninteracting particles, the measured correlation function, $C(q,\tau)$, needs to be inverted to obtain a corresponding distribution of diffusion coefficients [or hydrodynamic diameters from Eq. (3)], a challenging mathematical inverse-problem (see Refs. 44-49). Various methods have been developed to extract the size distribution from the measured correlation function, and algorithms of these methods have been written into routine software packages such as those provided by Brookhaven Instruments Corp., Holtsville, New York. In particular, we use CONTIN, a constrained regularization method for inverting data represented by linear algebraic or integral equations, which was developed by Provencher[46] to analyze data from polydisperse solutions. For a rapid assessment of the early stage of aggregation/polymerization of DoTu rings we apply the cumulant method, in which the measured correlation function is fit with the following expansion,[49]

$$\mathrm{Ln}[C(q,\tau) - 1]^{1/2} = \mathrm{Ln}(B)^{1/2} - \overline{D}q^2\tau + \frac{\mu}{2}\tau^2 \ldots \qquad (4)$$

where the first term on the right-hand side is a constant determined experimentally, $\overline{D}$ is an average diffusion coefficient, and $\mu$ is related to the width of the size distribution. In accordance with Eq. (3) we can determine an average hydrodynamic diameter, $\overline{d}_H$. By measuring correlation functions at various times during the experimental period we can monitor possible changes of $\overline{d}_H$ and thereby obtain insight into changes of the sample due to assembly/disassembly or aggregation.

In the analysis of the DLS and SV of the CrTu and DoTu samples, it is important to consider the interparticle interactions of such assembly/disassembly systems under the studied conditions. First, the initial concentrations of tubulin and cryptophycin or dolastatin are high enough to assure ring formation as described in *Samples* section. Second, a systematic study of CrTu and DoTu ring stability upon dilution shows that both the CrTu and DoTu samples appear stable at 100 n$M$ concentration, indicating that the micromolar concentrations used in the DLS measurements are appropriate and above the critical assembly/disassembly concentration of the rings for both samples. Third, given the low concentration ([Tu] $\sim$ micromolar) of the samples, it is reasonable to neglect the hydrodynamic effects due to interparticle interactions in the analysis of the DLS and SV measurements as well as in the FCS measurements (see below). However, thermodynamic effects, which involve ring-ring interactions and formation of large structures such as the case in the DoTu, cannot be ignored. These effects can be readily observed in the measured DLS correlation functions as well as in the SV profiles. It is, however, difficult to extract an accurate distribution of the size in the sample. Instead, we have attempted to quantify the growth kinetics of the large structures, which likely are stacks of rings as shown by SANS (see *Small-Angle Neutron Scattering* section).

***DLS: Cryptophycin-Tubulin.*** The beam of an Argon laser ($\lambda$ = 488 nm) was collimated and focused onto the sample. The scattered photons were collected at various angles by an EMI-PMT Model 9863 photon counting tube, transformed by a discriminator-amplifier into TTL pulses, and then processed by a BI-9000AT correlator board (Brookhaven Instruments Corp.) to generate intensity–intensity time correlation functions. The sample, loaded in a glass cell, was placed in a decalin index-matching bath attached to a precision goniometer (Brookhaven Instruments). The temperature of the bath was set to (22.0 $\pm$ 0.1)°C.

We collected several correlation functions from CrTu samples at various scattering angles (60°, 90°, and 120°). In Figure 4a we plot a typical autocorrelation function at a 90° scattering angle, along with the intensity-weighted distribution of the hydrodynamic diameter as extracted by the CONTIN method (see inset). The later suggests the presence of two components in the sample. The first peak can be attributed to the CrTu rings with a weighted average hydrodynamic diameter, $\overline{d}_H = 24 \pm 4$ nm, the error being the standard deviation. This value is similar to that determined from the value of the diffusion coefficient ($\overline{D} = 1.8 \times 10^7$ cm$^2$/s) reported in Ref. 8, but somewhat larger than the value determined by FCS, where a single-component fit is satisfactory (see below, and Ref. 10). The widths of the peaks generally do not faithfully represent sample characteristics but contain artifacts attributable to the inversion method (CONTIN), which tends also to be sensitive to slowly varying components of $C(q,\tau)$ linked to small amounts of aggregated material. It is difficult to assess the accuracy of the distribution derived with the method, especially when several size distributions are present. In the particular case of our closed-ring polymers one can certainly argue that the width of the first peak is misleading, as it suggests that the sample contains rings with different numbers of tubulin dimers. This is incorrect, as demonstrated in Ref. 11 where we combined SV and FCS to show that the CrTu rings overwhelmingly contain eight tubulin dimers. We surmise that the second broad peak in Figure 4a is likely due to aggregates of tubulin, although we cannot rule out other entities. A similar peak was detected by SV but not by FCS.[10,11] Note that because aggregates scatter roughly in proportion to the square of their mass the amount of material in the larger structures actually is much less than appears in Figure 4a.

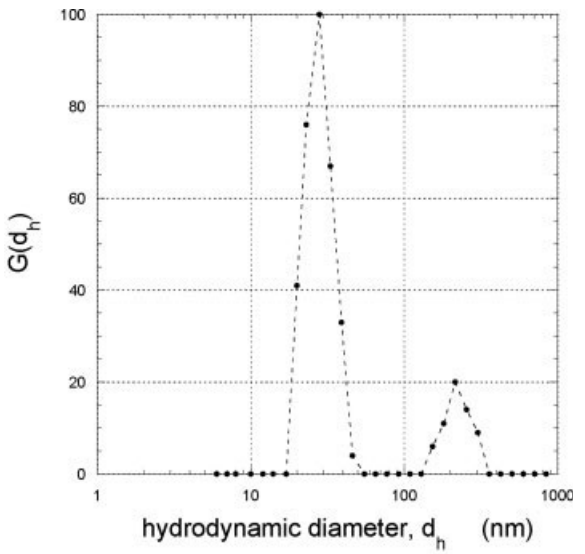


**FIGURE 4** (a) Size distribution of CrTu samples derived from measured DLS correlation functions using CONTIN. The first major peak is attributed to the rings but the source for the second small peak is unknown. (b) Changes of the average hydrodynamic diameter, $\overline{d}_H$, of entities in DoTu samples derived from analysis of DLS correlation functions with cumulant method [see Eq. (4)].

If we use the Nxbead model, we calculate the expected hydrodynamic diameter to be $d_H$(16bead) = 19.6 nm, where we take $N = 16$ and $a = 4.75$ nm (diameter) to be consistent with the values derived from the SANS data (see *Small-Angle Neutron Scattering* section). With the 21-minibead model, we compute a value $d_H$ (16 × 21minibead) = 22.2 nm, which is closer to the experimental DLS value. These calculated values are lower than that obtained from DLS ($\overline{d}_H = 24 \pm 4$ nm) but, for the reasons discussed above, the latter has only limited accuracy. We show, below, how, by combining FCS measurements on tubulin monomers with measurements on rings, one can determine which model best represents the ring structures [see discussion above Eq. (12)].

***DLS: Dolastatin-Tubulin.*** In contrast to the CrTu samples, which were stable, it was difficult to determine accurately the hydrodynamic diameter of the DoTu rings because of the rapid formation of large supramolecular structures in the samples. We used DLS to monitor the formation of these large macrostructures by measuring correlation functions at

various times following the mixing of tubulin and dolastatin in the buffer. Given the good signal-to-noise ratio, we collected a sequence of 1 to 2-min correlation functions. Using the cumulant method [Eq. (4)] we determined changes in the average hydrodynamic diameter with time as shown in Figure 4b. The figure indicates the relatively fast aggregation or self-assembly process of the rings.

Using the two models we calculate the corresponding hydrodynamic diameters for DoTu to be $d_H = 30.1$ nm for the 28Xbead ring with a 4.75 nm bead diameter and $d_H = 32.4$ nm for the 28 × 21-minibead ring; we set $N = 28$ for consistency with the SANS results (see earlier section). However, these calculated values are small compared with the average diameters (∼48 nm) measured in the early stage ($t < 4$ min; see Figure 4b). This apparent discrepancy can be attributed to the formation of the large structures in the samples, which tend to affect the measured correlation functions. That is, the sample is no longer composed of monodisperse particles (rings only); rather large structures (which, based on SANS results, likely are stacks of rings—see *Small-Angle Neutron Scattering* section) contribute significantly to the scattering, inducing deviations from one-component correlation functions. It appears the aggregation/polymerization of the rings is too fast to follow, despite our efforts to rapidly place the sample in the DLS instrument (few minutes at most).

## Sedimentation Velocity

Sedimentation velocity experiments were conducted in a Beckman Optima XL-I/A analytical ultracentrifuge (Beckman Coulter, Fullerton, CA) at two different rotor speeds of 25,000 and 50,000 rpm, and at fixed temperature. The differential refractive index distribution across the solution column was measured using the laser interferometry imaging system of the analytical ultracentrifuge as explained in Refs. 50–55.

We analyze the centrifugation data with an expression describing the time-dependent sedimentation and diffusion of a single species with concentration, $\chi(r,t)$, in the centrifugal field. That is, we use the Lamm equation,[51]

$$\frac{\partial \chi}{\partial t} = \frac{1}{r}\frac{\partial}{\partial r}\left(rD\frac{\partial \chi}{\partial r} - s\omega^2 r^2 \chi(r)\right), \tag{5}$$

where $r$ denotes the radial distance from the center of rotation, $\omega$ the rotor angular velocity, $s$ the macromolecular sedimentation coefficient, and $D$ the translational diffusion coefficient. Both $s$ and $D$ depend strongly on the molar mass, $M$, and are related by the Svedberg equation,[50]

$$S = \frac{\mathrm{MD}(1 - \bar{v}\rho)}{\mathrm{RT}} \tag{6}$$

where $\bar{v}$ is the partial specific volume, $\rho$ the density of the solvent, $T$ the temperature, and $R$ the gas constant. For polydisperse solutions, several methods have been developed to invert measured centrifugation profiles, similar in essence to the treatment of DLS data. Here, we apply the software SEDPHAT (see website in Ref. 55).

Because polymerization of tubulin is expected to proceed with the formation of a finite number of tubulin polymers, we developed and implemented a procedure where we first inverted the centrifugation data using a continuous (unknown) distribution $C(s)$, followed by refinement with a sum of functions associated with a discrete distribution of tubulin oligomers (i.e. monomers, dimers, trimers, etc.). The maximum entropy method was introduced to optimize the inversion and to determine the likely $n$-mers available in the sample. In Figure 5 we show the $C(s)$-distributions corresponding to the centrifugation profiles of the Tu and CrTu samples. Figure 5 shows a pronounced peak at $s = 5.5$ Svedberg for the Tu sample and, in contrast, a pronounced peak at $s = 15.9$ Svedberg for the CrTu sample, which can be at first glance ascribed to 8-dimer rings. In addition, a small peak ($s \sim 5.5$ Svedberg) is discerned in the CrTu sample

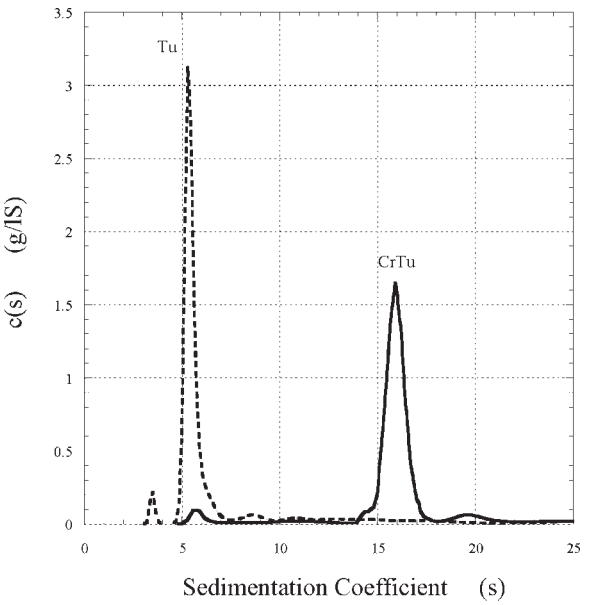


**FIGURE 5** Measured distribution of sedimentation coefficients of tubulin (dashed line) and cryptophycin-tubulin (solid line) samples ([Tu] = 5 $\mu M$; [Cryptophycin] = 8 $\mu M$ in MES buffer). Each peak is identified with the corresponding entities: tubulin dimers (Tu) or tubulin rings (CrTu). Note that there are no measurable intermediate oligomers between tubulin and cryptophycin-tubulin rings in the CrTu sample.

that appears to be compatible with the major peak of the Tu sample, indicating the presence of a small amount of unpolymerized tubulin in the CrTu sample. Also note a relatively broad but small peak at $s = 20$ Svedberg, which may be due to aggregates of tubulin rings or other unknown entities (see also Figure 4a). More interestingly, Figure 5 indicates that, under the studied conditions, there are no substantial amounts of stable oligomers intermediate between the tubulin dimers and the ring polymers in the CrTu sample. The optimization procedure yields rms errors comparable with the noise of the data acquisition, allowing us to extract the following ratio, $\sigma = s(\text{CrTuRing})/s(\text{TuDimer}) = 2.89 \pm 0.02$, of the sedimentation coefficients of the CrTu rings and the Tu dimers.[11] This ratio will be compared below with related ratios derived from FCS measurements and calculations.

## Fluorescence Correlation Spectroscopy

Our experimental FCS setup is described elsewhere.[56–58] In contrast to DLS, FCS utilizes temporal fluctuations in fluorescence intensity rather than scattering to obtain information about particle motions occurring within a small excitation volume. Fluorescence intensities, $i(t)$, acquired sequentially at times, $t$, are time-correlated to generate a correlation function as defined in Eq. (1). The excitation volume is made small (femtoliter to subfemtoliter) by either confocal geometry or by multiphoton excitation.[56] Typically, samples containing nanomolar concentrations of particles are probed. For noninteracting, freely diffusing, fluorescent particles with different translational diffusion coefficients and brightness, a closed-form expression of Eq. (1) can be derived:[59–63]

$$G(r) = 1 + \frac{1}{\left(\sum_{j=1} n_j Q_j\right)^2} \sum_{i=1} \frac{n_i Q_i^2}{(1+\tau/\tau_{di})(1+p\tau/\tau_{di})^{1/2}}. \quad (7)$$

In Eq. (7), $n_i$ denotes the average number of fluorescent particles of type $i$ in the excitation volume, $Q_i$ the fluorescence quantum yield of the particles, and $\tau_{di}$ the diffusion time of the particles as defined below. In the derivation of Eq. (7) it is assumed that the fluorescent particles are excited by a three-dimensional Gaussian beam, $W(r,z) = C \exp[-2(r/r_0)^2]\exp[-2(z/z_0)^2]$, characterized by two length scales, $r_0$ and $z_0$, defined in the focusing plane and the optical axis along the direction of the laser beam, respectively. With such an idealized Gaussian beam, $\tau_{di} = (r_0)^2/4D_i$, $D_i$ being the translational diffusion coefficient. Also, in Eq. (7), $P = (r_0/z_0)^2$ is an instrumental constant set by the width of the incident beam and the size of the confocal setup.

From measured correlation functions, two features typically can be identified. First is the limiting value ("the amplitude") of the correlation function:

$$A = G(0) - 1 = \frac{\sum_i n_i Q_i^2}{\sum_j (n_j Q_j)^2}, \quad (8)$$

which depends on the variation in the brightness of the particles. Only in the limits $Q_i$ = constant or $Q_i \to \infty$ does the amplitude depend solely on the number of particles.

Second is the set of diffusion times, $\{\tau_{di}\}$, which can be alternatively expressed in terms of the hydrodynamic diameter, $\{d_{Hi}\}$, using the Stokes-Einstein relation in Eq. (3). In principle, these diffusion times can be extracted by fitting the measured correlation function with the expression in Eq. (7), with the various $n_i$, $Q_i$, and $\tau_{di}$ being the unknown parameters. This procedure is not straightforward because of the large number of fitting parameters, involving a mathematical inverse problem that is challenging to solve.[59–62] In practice, to accurately fit Eq. (7) with even two species of fluorescent particles is a daunting task (at least four fitting parameters). This is significantly simplified if one has a priori knowledge of some of the parameters, e.g., the diffusion coefficient of one or both of the constituents. When only one species is present, Eq. (7) reduces to:

$$G(\tau) = 1 + \frac{1}{n} \frac{1}{(1+\tau/\tau_d)(1+p\tau/\tau_d)^{0.5}}, \quad (9)$$

where we have assumed, here, that all particles have the same brightness. The prefactor, $n$, denotes the average number of particles per unit volume.[58]

***FCS: Tu, Cryptophycin-Tubulin, Dolastatin-Tubulin.*** In Figures 6a and 6b we plot correlation functions collected from samples of tubulin (Tu), cryptophycin-tubulin (CrTu), and dolastatin-tubulin (DoTu), all prepared and handled under the same conditions. Based on the fluorescence intensities the concentrations of Tu, CrTu, and DoTu samples were 100, 120, and 28 n$M$, respectively. Because of the formation of large aggregates, and subsequently removal by a Millipore filter (200 $\mu$m), the concentration of tubulin in the DoTu sample is much lower than the initial 100 n$M$ concentration. Two characteristics of the curves in Figures 6a and 6b indicate polymerization of the tubulin into rings. First, in Figure 6a we focus on the amplitude, $(G(\tau \to 0) - 1) = A$, of the curves. If all Tu, CrTu, and DoTu samples had equal total mass of identically labeled tubulin, we would expect the ratios of the amplitudes of the correlation functions to be

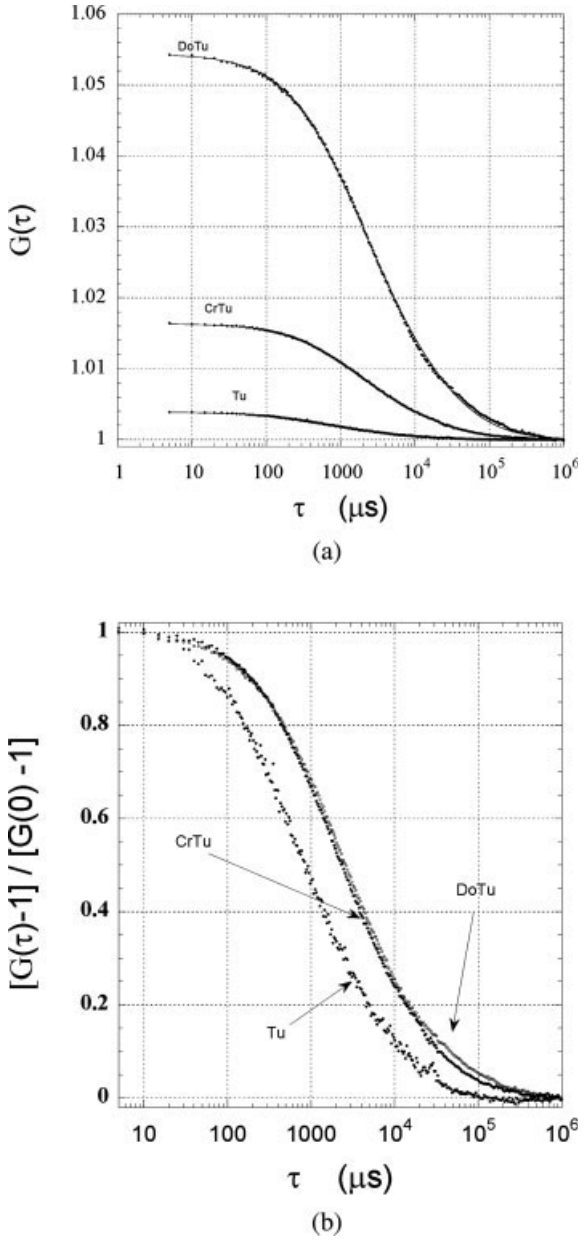


**FIGURE 6** (a) Measured FCS correlation functions and fitted curves of tubulin (Tu), cryptophycin-tubulin (CrTu), and dolastatin-tubulin (DoTu) samples are shown as a function of the delay time, $\tau$. (b) The correlation functions shown in Figure 6a are normalized to unity in order to highlight the shift in the diffusion time caused by the polymerization of the tubulin dimers when mixed with cryptophycin or dolastatin.

A(CrTu)/A(Tu) = 8 and A(DoTu)/A(Tu) = 14, respectively, following the polymerization of the tubulin dimers into isolated rings [cf. Eq. (9) and earlier discussion]. However, A(CrTu), A(DoTu), and A(Tu) depend on the actual numbers of fluorescent particles in the CrTu, DoTu, and Tu samples and their corresponding brightness. If the chemical labeling protocol produces a Poisson distribution for the brightness of tubulin, the amplitude of the correlation function in Eq. (8) can be simplified to:

$$A = G(0) - 1 = \frac{1}{\sum_i n_i}\left(1 + \frac{1}{\overline{m}}\right) \tag{10}$$

where $\overline{m}$ is the average number of fluorophores per tubulin dimer and $\sum_i n_i$ is the total number of particles in the illuminated volume (where here the index $i$ refers to particles of differing brightness). If all of the tubulin dimers in the peptide-tubulin sample polymerize into rings and the Poisson labeling distribution is preserved with $\overline{m}(\text{ring}) = (N/2) \times \overline{m}(\text{dimer})$ where $N$, as above, signifies the number of monomers, then the ratio of the amplitude of the correlation functions of the primary tubulin and the polymerized peptide-tubulin samples is expected to be:

$$\frac{\text{A(CrTu)}}{\text{A(Tu)}} = \frac{1 + (N/2)\overline{m}}{1 + \overline{m}}. \tag{11}$$

In our tubulin samples, $\overline{m} \approx 1$, so, we expect A(CrTu)/A(Tu) = 4.5 for the CrTu rings and 7.5 for the DoTu rings. These calculated values need to be compared with the experimental values: A(CrTu)/A(Tu) = 5.0 and A(DoTu)/A(Tu) = 4.0, respectively (both measured ratios were corrected for the tubulin concentrations of the corresponding samples; [Tu] 100 n*M*, [CrTu] = 120 n*M*, and [CrTu] = 28 n*M*). There is certainly close agreement between the measured (5.0) and calculated (4.5) values for the CrTu sample. However, for the case of DoTu, there is poor agreement (calculated (7.5) vs. measured (4.0)). This disagreement is due to the polydispersity in brightness of the fluorescent particles in the DoTu sample, which contains not only DoTu rings but also unpolymerized tubulin (see discussion below) and large structures as mentioned above (see also SANS data). As a result, the brightness of the individual particle affects differentially the measured amplitude of the DoTu correlation function [see Eq. (8)].

Second, in Figure 6b we show the correlation functions normalized to unity to indicate the shift of the diffusion times to longer times upon the polymerization of the tubulin dimers. The CrTu correlation curve is shifted uniformly with respect to that of the Tu curve, indicating a uniform change of the size from tubulin to tubulin polymers. That is, the size distribution of the CrTu polymers is relatively narrow, which is confirmed by the markedly good fit of the data with an expression for one-component system [see Eq. (9)]. From the fit we have determined the ratio of the diffusion times to be: $\tau_d(\text{CrTu})/\tau_d(\text{Tu}) = 2.75$.

In the case of DoTu samples, the DoTu correlation curve is not shifted uniformly with respect to the Tu curve, suggesting polydispersity of the sample. By assuming the DoTu sample to be composed of two main components, tubulin dimers and oligomers (likely rings), we have determined the following ratio of the diffusion times: $\tau_d(\text{DoTu})/\tau_d(\text{Tu}) = 4.0$, $\tau_d(\text{DoTu})$ being the diffusion time of individual dolastatin-tubulin rings. It should be noted that the presence of larger entities introduces a small systematic deviation in the fit at longer times ($\tau > 10^4$ $\mu$s).

For comparison with measurements we calculate the ratio of the hydrodynamic diameters (equivalent to diffusion times), $d_H(\text{ring})/d_H(\text{dimer})$, of a ring polymer and a dimer as a function of the number of monomers. These calculations are performed for both structural models shown in Figure 2. In Figure 7 we plot the results as well as the measured ratios of the diffusion times derived from the Tu, CrTu, and DoTu samples. The figure indicates that when the asymmetric shape of the tubulin monomer is taken into account (i.e. 21-minibead representation), we find consistent agreement between the measurements and the calculations. Remarkably, the measured ratios from the CrTu and DoTu samples fall very close to the computed curve when $N$ is set to 16 or 28, respectively, consistent with the known values for CrTu and DoTu rings. This suggests that FCS, which probes the hydrodynamic behavior of particles in solutions, is able to resolve the basic asymmetric shape of the nanoscopic tubulin monomer.

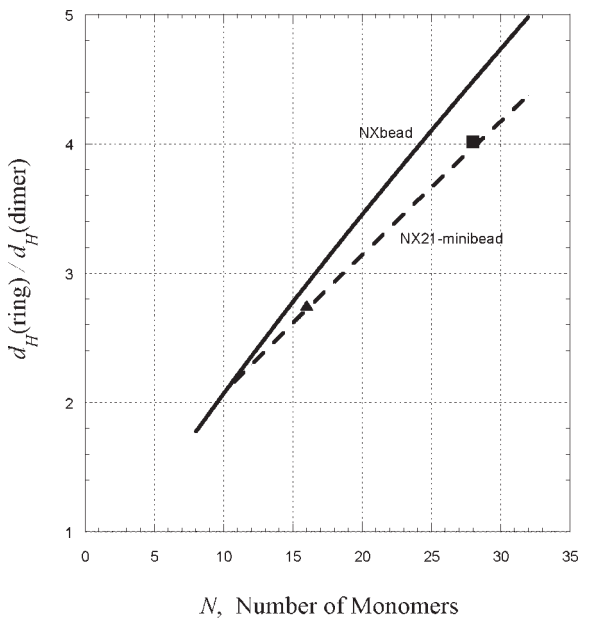


**FIGURE 7** Calculated ratios of the hydrodynamic diameter of rings made with $N$ monomers to that of isolated dimers are shown as a function of $N$. The monomer is represented either by a spherical bead (solid line) or 21-minibeads (dashed line) (see Figure 2). The ratios derived from FCS correlation functions measured on tubulin, cryptophycin-tubulin (CrTu, ▲), and dolastatin-tubulin (DoTu, ■) samples fall close to the dashed curve, indicating that the 21-minibead model is a better representation of tubulin monomers.

***Consistency Between FCS and SV Data.*** A useful comparison between the SV and FCS data can be derived from the ratio of the Svedberg coefficients of the tubulin dimer and 8-dimer rings [see Eq. (6)]:

$$\sigma = \frac{s(\text{CrTu})}{s(\text{Tu})} = \frac{M(\text{CrTu})}{M(\text{Tu})}\frac{D(\text{CrTu})}{D(\text{Tu})} = \frac{M(\text{CrTu})}{M(\text{Tu})}\frac{\tau_d(\text{Tu})}{\tau_d(\text{CrTu})} \quad (12)$$

where the functional forms, $s(..)$, $M(..)$, $D(..)$, $\tau(..)$, denote the parameters of the corresponding tubulin dimers (Tu) or rings (CrTu). If we set the ratio $M(\text{CrTu})/M(\text{Tu}) = 8$ (neglecting the mass of cryptophycin), we end up with a relation that relates the ratio of the Svedberg coefficients determined from SV measurements to the ratio of the diffusion times determined independently from FCS measurements. From SV measurements we have determined $s(\text{CrTu})/s(\text{Tu}) = 2.88$, which agrees very well with the ratio $8\tau_d(\text{CrTu})/\tau_d(\text{Tu}) = 2.91$, determined from FCS measurements.

In the case of DoTu samples we did not find a need to perform a thorough global analysis of the SV data similar to that of CrTu samples. By using the average SV value published in Table I in Ref. 8: $s(\text{DoTu}) = 20$ S, we found a good agreement between the SV data and those of FCS. Similarly to Eq. (12), we derive the following equality between the ratio of the Svedberg coefficients and that of the diffusion times of the Tu dimers and DoTu rings:

$$\sigma = \frac{s(\text{DoTu})}{s(\text{Tu})} = \frac{M(\text{DoTu})}{M(\text{Tu})}\frac{D(\text{DoTu})}{D(\text{Tu})} = \frac{M(\text{DoTu})}{M(\text{Tu})}\frac{\tau_d(\text{Tu})}{\tau_d(\text{DoTu})}, \quad (13)$$

where we set $M(\text{DoTu})/M(\text{Tu}) = 14$, yielding the following value $s(\text{DoTu})/s(\text{Tu}) = 3.64$ for the left-hand side of the SV part of Eq. (13) which is close to the value of 3.49 for the right-hand side of the equation. However, the agreement is not as good as that of the CrTu samples where the value of the ratio of the SV data was determined from a global fit of the data.

## SUMMARY

The present results show the suitability of using complementary SANS, DLS, SV, and FCS to probe cryptophycin-tubulin

and dolastatin-tubulin ring polymers in solution. A common thread to all these techniques is their appropriateness for characterizing nanoscopic structures. The techniques are relatively nonintrusive and provide direct insight into the polymerization of the peptide-tubulin complexes. Different concentration criteria apply, however, for each technique. Because of the weak scattering of neutrons by proteins, the SANS samples were prepared at relatively high concentrations ([Tu] = 40 $\mu M$) in order to have a good signal-to-noise level. Several peaks and humps are readily discernable on the scattering profiles of both samples (Figure 3a). For CrTu samples the main characteristics of the measured SANS profiles can be readily reproduced by the two models shown in Figure 2 with the number of monomers set to 16 (eight tubulin dimers/ring). SANS is seen to be appropriate for confirming the structure of isolated rings. Moreover, this technique is unique in providing information about the internal ordering of the large macrostructures formed in the DoTu solutions. The profiles of the DoTu samples show pronounced peaks that could not be accounted for by either of ring models shown in Figure 2. Light scattering crudely indicates the presence of relatively large structures in these samples, but SANS allows one to infer the internal geometries of those entities. We suggest a stacking mechanism of the rings, which is consistent with the detailed features of the observed scattering cross-sections.

For DLS and SV measurements, the samples were prepared with reduced concentrations ($\sim 4\mu M$), an order of magnitude less than those for SANS. In the case of CrTu samples, both SV and DLS indicate the presence of not only the rings but also a small amount of larger entities. We find that the measured DLS hydrodynamic diameter is consistently larger than that calculated from both models shown in Figure 2. This apparent discrepancy may be due to large entities, which introduce inaccuracy in the size distribution when inverting the DLS correlation functions. SV has provided significant insight into the polymerization of the peptide-tubulin complexes. Indeed, under the studied conditions, SV data indicate that no substantial amount of stable intermediate oligomers coexist with the CrTu rings. It is important to note a virtue of SV technique, namely, separation of signal due to rapid sedimentation of large entities that reduces their effect on the analysis of the data. In contrast, all entities contribute to, and are intermixed in, the overall signal obtained by DLS.

A primary interest in FCS is its suitability for applications to solutions of fluorescent probes at nanomolar concentrations. This optical technique is particularly attractive in situations involving costly or rare materials, and also allows one to look at sample concentrations low enough that self-association of target molecules is minimized. We have successfully applied FCS to investigate the hydrodynamic behavior of labeled tubulin dimers and of tubulin ring polymers induced by interactions of tubulin with cryptophycin or dolastatin. The FCS measurements of the CrTu samples at these low concentrations yield unequivocal characteristics of the CrTu rings. By verifying Eqs. (12) and (13), we demonstrated that FCS and SV yield consistent measurements that are appropriate to identify and characterize the various polymeric structures in vitro.

Until now there has been no high-resolution experimental study of circular ring polymers in solution because of difficulties in obtaining appropriate samples for experimental studies.[32,33] We have exploited the attributes of these tubulin rings to test available hydrodynamic theories of supramolecular structures and have shown that related calculations of hydrodynamic coefficients are quantitatively correct, especially with the three-dimensional, 21-minbead representation of a tubulin monomer. This representation also appears to account well for the three-dimensional structure of the CrTu and DoTu rings. In particular, calculated scattering profiles and values for the translational diffusion coefficient are in close agreement with those measured by SANS and FCS. This result provides additional evidence for the validity of the methodologies developed for calculating the static and hydrodynamic properties of supramolecular nanoscopic structures.

This work was supported by intramural funds from the National Institute of Child Health and Human Development, NIH.

## REFERENCES

1. Alberts, B.; Bray, D.; Lewis, J.; Raff, M.; Roberts, K.; Watson, J. D. Molecular Biology of the Cell, 3rd ed.; Garland Publishing: New York, 1994.
2. Nogales, E.; Whittaker, M.; Milligan, R. A.; Downing, K. H. Cell 1999, 96, 79–88.
3. Bordas, J.; Mandelkow, E. M.; Mandelkow, E. J. Mol Biol 1983, 164, 89–135.
4. Diaz, J. F.; Pantos, E.; Bordas, J.; Andreu, J. M. J Mol Biol 1994, 238, 214–223.
5. de la Torre, J. G.; Andreu, J. M. J Mol Biol 1994, 238, 223–225.
6. Prasad, V.; Jordan, M. A.; Luduena, R.F. J Protein Chem 1992, 11, 509–515.
7. Hamel, E.; Covell, D. G. Curr Med Chem Anti-Cancer Agents 2002, 2, 19–53.
8. Watts, N. R.; Cheng, N.; West, W.; Steven, A. C.; Sackett, D. L. Biochemistry 2002, 41, 12662–12669.
9. Watts, N. R.; Sackett, D. L.; Ward, R. D.; Miller, M. W.; Wingfield, P. T.; Stahl, S. S.; Steven, A. C. J. Cell Biol 2000, 150, 349–360.
10. Boukari, H.; Nossal, R.; Sackett, D. Biochemistry 2003, 42, 1292–1300.
11. Boukari, H.; Nossal, R.; Sackett, D.; Schuck, P. Phys Rev Lett 2004, 93, 98106.

12. Boukari, H.; Chernomordik, V.; Krueger, S.; Nossal, R.; Sackett, D. Physica B 2004, 350, e533.
13. Panda, D.; Himes, R. H.; Moore, R. H.; Wilson, L.; Jordan, M. A. Biochemistry 1997, 36, 12948–12953.
14. Pettit, G. R.; Kamano, Y.; Herald, C. L.; Tuinman, A. A.; Boettner, F. E.; Kizu, H.; Schmidt, J. M.; Baczynskyj, L.; Tomer, K. B.; Bontems, R. J. J Am Chem Soc 1987, 109, 6883–6885.
15. Dumontet, C.; Sikic, B. I. J Clin Oncol 1999, 17, 1061–1070.
16. Bai, R.; Taylor, G. F.; Cichacz, Z. A.; Herald, C. L.; Kepler, J. A.; Pettit, G. R.; Hamel, E. Biochemistry 1995, 34, 9714–9721.
17. Bai, R.; Pettit, G. R.; Hamel, E. Biochem Pharmacol 1990, 39, 1941–1949.
18. Hud, N. V.; Downing, K. H. Proc Natl Acad Sci USA 2001, 98, 14925–14930.
19. Zhang, A.; Wassarman, K. M.; Ortefa, J.; Steven, A.C.; Storz, G. Mol Cell 2002, 9, 11–22.
20. Kuriyan, J.; O'Donnell, M. J Mol Biol 1993, 234, 915–925.
21. VanLoock, M. S.; Kasai, M.; Yu, X.; Egelman, E. H. J Struct Biol 2001, 135, 58–66.
22. Hinshaw, J. E.; Schmid, S. L. Nature 1995, 374, 190–192.
23. Edeling, M. A.; Smith, C.; Owen, D. Nat Rev Mol Cell Biol 2006, 7, 32–44.
24. Nossal, R. Traffic 2001, 2, 138–147.
25. Zlotnick, A. J Mol Biol 1994, 241, 59–67.
26. Zlotnick, A. J Mol Recognit 2005, 18, 479–490.
27. Gurkan, C.; Stagg, S. M.; Lapointe, P.; Balch, W. E. Nat Rev Mol Cell Biol 2006, 7, 727–738.
28. Stagg, S. M.; Gurkan, C.; Fowler, D. M.; LaPointe, P.; Foss, T. R.; Potter, C. S.; Carragher, B.; Balch, W. E. Nature 2006, 439, 234–238.
29. Antonny, B.; Gounon, P.; Schekman, R.; Orci, L. EMBO Rep 2003, 4, 419–424.
30. Behrens, S.; Habicht, W.; Wagner, K.; Unger, E. Adv Mater 2006, 18, 264–289.
31. Mitra, A.; Sept, D. Biochemistry 2004, 43, 13955–13962.
32. Leish, T. Science 2002, 297, 2005–2006.
33. Bielawski, C. W.; Benitz, D.; Grubbs, R. H. Science 2002, 297, 2041–2044.
34. Obukhov, S.; Rubinstein, M.; Duke, T. Phys Rev Lett 1994, 73, 1263–1266.
35. de La Torre, J. G.; Navarro, S.; Martinez, M. C. L.; Diaz, F. G.; Cascales, J. L. Biophys J 1994, 67, 530–531.
36. de La Torre, J.G.; Bloomfield, V.A. Quarterly Rev Biophys 1981, 14, 81–139.
37. Hubbard, J. B.; Douglas, J. F. Phys Rev E 1993, 47, 2983–2986; and references therein.
38. Yamakawa, H.; Yamaki, J. I. J Chem Phys 1973, 58, 2049–2055.
39. http://www.stevens.edu/zeno/.
40. Kostorz, G. Neutron Scattering; Academic Press: New York, 1979.
41. Glinka, C. J.; Rowe, J. M.; LaRock, J. G. J Appl Cryst 1985, 19, 427–439.
42. Glinka, C. J.; Barker, J. G.; Hammouda, B.; Krueger, S.; Moyer, J. J.; Orts, W. J. J Appl Cryst 1998, 31, 430–445.
43. Berne, B. J.; Pecora, R. Dynamic Light Scattering; Wiley: New York, 1976.
44. Nossal, R. Methods Exp Phys 1982, 20, 299–336.
45. Provencher, S. W. Biophys J 1976, 16, 27–41.
46. Provencher, S. W. Comput Phys Commun 1982, 27, 229–242.
47. Morrison, I. D.; Grabowski, E. F.; Herb, C. A. Langmuir 1985, 1, 496–501.
48. Nyeo, S.-L.; Chu, B. Macromolecules 1989, 22, 3998–4009.
49. Koppel, D. E. J. Chem Phys 1972, 57, 4814–4820.
50. Svedberg, T.; Pederson, K. O. The Ultracentrifuge; Oxford University Press: London, 1940.
51. Lamm, O. Ark Mat Astr Fys 1929, 21B, 1–4.
52. Schuck, P. Biophys J 2000, 78, 1606–1619.
53. Schuck, P.; Perugini, M. A.; Gonzales, N. R.; Howlett, G. J.; Schubert, D. Biophys J 2002, 82, 1096–1111.
54. Schuck, P.; Demeler, B.; Biophys J 1999, 76, 2288–2296.
55. www.analyticalultracentrifugation.com/references.htm.
56. Webb, W. W. Appl Opt 2001, 40, 3969–3983.
57. Rigler, R.; Elson, E. S. Fluorescence Correlation Spectroscopy: Theory and Applications (Springer Series in Chemical Physics); Springer-Verlag, New York, 2001.
58. Chen, Y.; Müller, J. D.; Berland, K. M.; Gratton, E. Methods 1999, 19, 234–252.
59. Krichevsky, O.; Bonnet, G. Rep Prog Phys 2002, 65, 251–297.
60. Elson, E. L.; Magde, D. Biopolymers 1974, 13, 1–27.
61. Magde, D.; Elson, E. L.; Webb, W. W. Biopolymers 1974, 13, 29–61.
62. Aragon, S. R.; Pecora, R. J Chem Phys 1976, 64, 1792–1803.
63. Starchev, K.; Buffle, J.; Pèrez, E. J Colloid Interface Sci 1999, 213, 479–487.

*Reviewing Editor: Nils Walter*